Modeling of acoustic wave scattering from a two-dimensional fracture

Tianrun Chen, Mike Fehler, Steve Brown, Yang Zhang, Xingding Fang and Dan Burns, ERL Department of Earth, Atmospheric and Planetary Sciences, M.I.T, Ping Wang, CGGVeritas

Summary

In this paper, we model the acoustic scattering from a two dimensional fracture that is simulated by two different physical models. We calculate the scattering from the fractures with different properties based on these two models.

Introduction

We propose two possible representative models for a 2D fracture in reservoirs. The first one simulates the fracture as a low-aspect ratio *elliptical cylinder*. The inner properties of this elliptical cylinder are assumed to be homogeneous and different from the surrounding medium that is also homogenous. This model can approximately describe the actual shape of fractures observed in the field, and provides a clear physical sense of the distribution of the scattered energy over space. However, it lacks the detailed description of the fractures (micro fractures or cracks) and does not account for the effect of the rough contacting surfaces, which could greatly influence the stiffness or compliance of the fractures [Brown and Scholz (1985), Sevostianov et al., (2008), Romain et al., (2009)]. Ignoring these micro structures could result in an underestimation of the fracture stiffness. Our second model considers that a large fracture is composed of a sequence of smaller fracture. In this model the resulting fracture includes open and closed sections to capture some of the complexity of more realistic fracture geometries. Similar to the first model, the open crack sections are also modeled as low-aspect ratio elliptical cylinders, but with much smaller sizes.

Based on these two fracture models, the scattering from a fracture can be analytically calculated by matching the boundary conditions. These conditions are based on first principles and do not have any restrictions on the applicable frequency ranges or the size of the fractures. Also, these analytical expressions can be efficiently implemented in the frequency domain since each frequency component is independent from others and can be easily computed in parallel. This makes it easy to perform Monte-Carlo simulations and other statistical analysis to characterize the scattering from multiple fractures with random orientations, sizes, spatial distributions and inner properties.

There are several important practical applications of this analytical modeling method. ***First***, it provides a different perspective of waves propagate through fractures compared to a widely used finite-difference time-domain (FDTD) method based on Schoenberg's model [Schoenberg, (1980), Coates and Schoenberg, (1994), Willis et al., (2006)]. The signal received by receivers on the surface consists of two independent parts: the incident (source) wave field and the scattered wave field by fractures. It is important to analyze the scattered wave field independently since this part of the signal is sensitive to the properties of the fracture itself and also provides a way to understand the distribution of the scattered energy over space. It is not trivial for FDTD to decouple these two wave fields. However our analytical model can directly calculate the scattering from both single fractures and fracture networks. ***Second***, Schoenberg's model requires normal and tangential compliance as inputs. Until now, there are no *in-situ* measurements of these key parameters at the reservoir scale or direct evidence to justify which values should be used. The parameters in our analytical model are the velocities and densities of the surrounding medium as well as the medium inside the fractures, which could be determined from seismic measurements, well logging data or other measurements. Therefore, our analytical model could provide estimates of normal and tangential compliance by comparing the scattering calculated from Schoenberg's model with the one from the analytical model. ***Third***, this model, combined with the wave-number integration method, can be used to generate synthetic seismic data in a layered medium, which could potentially help (1) analyzing field data, (2) developing new inversion schemes for the properties of fracture networks, and (3) optimizing the source and receive positions and frequency range of future data acquisition.

Methodology

In this section, an analytical expression of the acoustic scattered field from an elliptical cylinder is formulated using an elliptic cylindrical coordinate system. The rectangular coordinates (x, y, z) is related to the elliptic cylindrical coordinates (u, v, z) via

$$\begin{aligned} x &= \frac{d}{2}\cosh u \cos v \\ y &= \frac{d}{2}\sinh u \sin v \\ z &= z, \end{aligned} \qquad (1)$$

where the half focus distance between F_1 and F_2 is given by $d/2 = \sqrt{a^2 - b^2}$, a and b are the semi- major and minor

axis of the ellipse respectively. The eccentricity is given by $e = d/2a$.

In order to match the boundary conditions where both the pressure and normal velocity need to be continuous along the boundary u, we need to decompose the incident wave $\phi(x, y)$ propagating in the plane (x, y) in terms of the elliptical waves. The plane wave $\varphi(x, y, z)$ propagating in a direction defined by the unit vector $\vec{n}(\sin\alpha\cos\beta, \sin\alpha\sin\beta, \cos\alpha)$ is

$$\begin{aligned}\varphi(x, y, z) &= e^{ik\sin\alpha(x\cos\beta + y\sin\beta)} e^{ikz\cos\alpha - i\omega t} \\ &= \phi(x, y) e^{ikz\cos\alpha - i\omega t}\end{aligned} \tag{2}$$

where ϕ is the plane wave propagated in plane (x, y) that can be decomposed in terms of elliptical waves [Stratton, (2007)]:

$$\begin{aligned}\phi &= e^{i\lambda(x\cos\beta + y\sin\beta)} \\ &= \sqrt{8\pi}\sum_m i^m \left[\frac{1}{N_m^e}\mathrm{Re}_m^1\left(\frac{d}{2}\lambda, u\right)\mathrm{Se}_m\left(\frac{d}{2}\lambda, v\right)\mathrm{Se}_m\left(\frac{d}{2}\lambda, \beta\right)\right. \\ &\quad \left. + \frac{1}{N_m^o}\mathrm{Ro}_m^1\left(\frac{d}{2}\lambda, u\right)\mathrm{So}_m\left(\frac{d}{2}\lambda, v\right)\mathrm{So}_m\left(\frac{d}{2}\lambda, \beta\right)\right]\end{aligned} \tag{3}$$

where $\lambda = k\sin\alpha$, Re_m^1 and Se_m are the m^{th} order of the first kind of even radial Mathieu functions and even angular Mathieu functions respectively, while Ro_m^1 and So_m are the m$^{\text{th}}$ order of the first kind of odd radial Mathieu functions and odd angular Mathieu functions respectively. The normalization constant $\frac{1}{N_m}$ is determined by the properties of the angular Mathieu functions. We can express the scattered field and field inside the elliptical cylinder in a similar way to the incident wave:

$$\begin{aligned}\phi^{sca} &= \sum_m i^m \left[A_m^e \mathrm{He}_m\left(\frac{d}{2}\lambda, u\right)\mathrm{Se}_m\left(\frac{d}{2}\lambda, v\right) + A_m^o \mathrm{Ho}_m\left(\frac{d}{2}\lambda, u\right)\mathrm{So}_m\left(\frac{d}{2}\lambda, v\right)\right] \\ \phi^{inn} &= \sum_m i^m \left[B_m^e \mathrm{He}_m\left(\frac{d}{2}\lambda, u\right)\mathrm{Se}_m\left(\frac{d}{2}\lambda, v\right) + B_m^o \mathrm{Ho}_m\left(\frac{d}{2}\lambda, u\right)\mathrm{So}_m\left(\frac{d}{2}\lambda, v\right)\right],\end{aligned} \tag{4}$$

where He_m and Ho_m are the third kind of even and odd radial Mathieu functions. The coefficients A_m and B_m are determined by matching the boundary conditions. In the far field, both He_m and Ho_m can be approximately written as

$$\mathrm{H}_m \approx \sqrt{\frac{2}{\pi}} \frac{e^{i(d/2)\lambda\cosh u} i^{-m}}{\sqrt{i(d/2)\lambda\cosh u}}. \tag{5}$$

We can express the far field scattered amplitude in terms of the scatter function $S(\frac{d}{2}\lambda, v, \beta)$

$$\phi^{sca} = S\left(\frac{d}{2}\lambda, v, \beta\right)\frac{e^{i(d/2)\lambda\cosh u}}{\sqrt{(d/2)\lambda\cosh u}}, \tag{6}$$

where the scatter function is

$$\begin{aligned}s\left(\frac{d}{2}\lambda, v, \beta\right) &= 4\sum_m Ae_m Se_m\left(\frac{d}{2}\lambda, v\right)e^{-i\frac{\pi}{4}} \\ &+ Ao_m So_m\left(\frac{d}{2}\lambda, v\right)e^{-i\frac{\pi}{4}}.\end{aligned} \tag{7}$$

Note that both A_m and B_m depend on the incident angle β. For the first model, we directly use Eq. (7) to calculate the scattering function (radiation pattern) of a single elliptical cylinder. This solution is exact and includes all interactions between the fracture and the wave field. For the second model, since the size of micro fractures are much smaller than the wave length, a low frequency approximation [Burke et al., (1963), Burke (1964)] to the radial and angular Mathieu functions is applied to calculate the scattering from each individual micro fracture through Eq. (7). The total scattered field is then the superposition of the contributions from all micro fractures. The multiple scattering between different micro fractures is assumed to be negligible compared to the single scattering. This is a reasonable assumption because (1) the amplitude of the multiple scattering is much smaller than the single scattering and the incident field and (2) the multiple scattering also tends to cancel each other due to the randomness of the micro fractures.

Results and Discussions

In this section, we first show the radiation patterns of a single elliptical fracture with different aspect ratios and inner properties. Then, we investigate the second model that simulates scattering from a series of micro fractures.

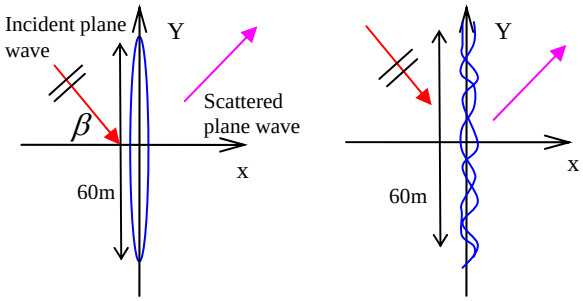

Figure 1: Geometry of the fracture (a) modeled as a single elliptical cylinder (2) composed of micro fractures, which are also modeled as elliptical cylinders. The surrounding

medium is homogeneous with P wave velocity 3000 m/s and density 2000 kg/m^3. The inner medium of the fracture is homogenous but with density 1800 kg/m^3 and differing P wave velocities. The incident plane wave propagates with $\beta = 45^o$. The total length of the fracture along the Y direction is 60 m. In the simulations, we will show how the radiation pattern changes as the inner P velocities and aspect ratios of the fractures change for a 100 Hz incident wave. Figure shows the radiation patterns for elliptical cylinders with the inner P wave velocity 2000 m/s but

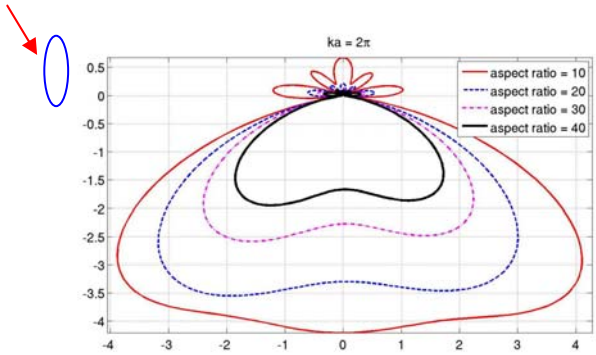

Figure 2 Radiation patterns of elliptical fractures with different aspect ratio.

with aspect ratio varying from 10 to 40. It is found that the forward scattering is much stronger than the backward scattering. As the aspect ratio increases, the amplitude of the scattering decreases because the size of the elliptical cylinder becomes smaller and more rigid as its width shrinks. The directionality, however, becomes stronger and the elliptical cylinder with aspect ratio 40 behaviors similarly to an array with a strong beaming along 45^o and 135^o. Figure 3 shows the radiation patterns for elliptical cylinders with a fixed aspect ratio 20 but with inner P velocity varying from 1000 m/s to 2500 m/s. Similar to Figure 2, the forward scattering is still much stronger than the backward scattering. As the impedance decreases, the amplitude of scattering decreases. When the frequency decreases to 50 Hz, the radiation patterns almost loses its directionality and becomes omni-directional in the forward direction, as shown in Figures 4 and 5. The radiation patterns are very similar for different aspect ratios and impedances but with different amplitudes.

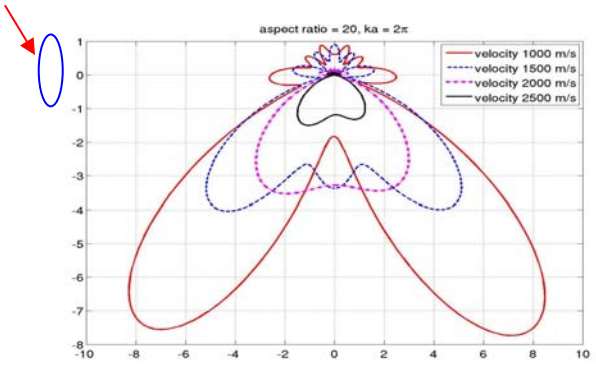

Figure 3 Radiation patterns of elliptical fractures with different inner P wave velocity and fixed aspect ratio 20.

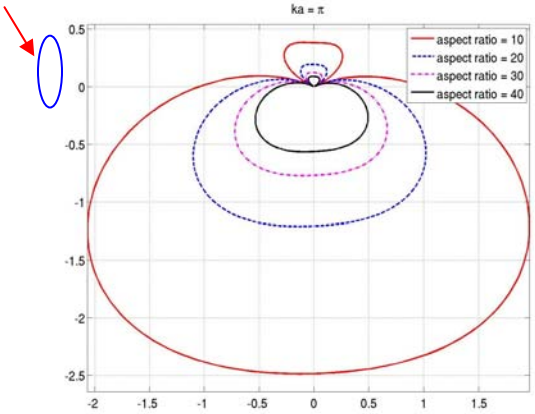

Figure 4: Similar to Figure 2, but for 50 Hz frequency

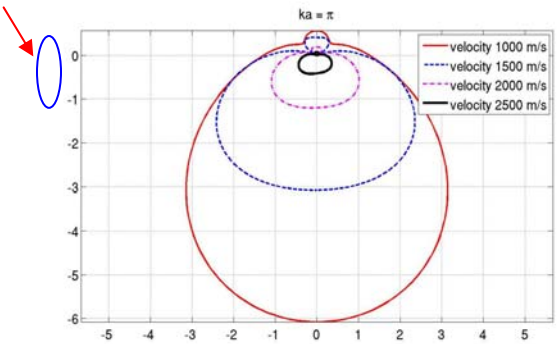

Figure 5 Similar to Figure 3, but for 50 Hz frequency.

All the above simulations are based on the first model which simulates the fracture as a single elliptical cylinder. Next, we show the results that are based on the second model in which the fracture is composed of many micro fractures that have different properties such as orientations, sizes, aspect ratios, long axis and inner P wave velocities. All of these properties can be estimated from geological data. In order to compare results with the first model, we assume that the fracture consists of identical micro fractures with 0.2 m long axes. Since the total length of the fracture is 60 m, there are a total of 300 micro fractures aligned together along the Y direction. Each micro fracture acts as a point scatterer since its size is about two orders of magnitude smaller than the wave length. Coherently superposing their contribution (single scattering) and ignoring their interaction (multiple scattering) results in an "array behavior" scattering of the whole fracture, as shown in Figure 7, which shows strong a beaming effect along 45^o and 135^o. A single elliptical cylinder also shows this array effect when the aspect ratio equals 40 as shown in Figure 2.

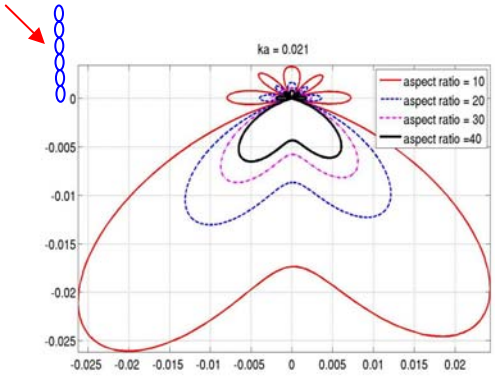

Figure 6 Radiation pattern for a fracture composed of identical micro fractures simulated as elliptical cylinders

Compared to the amplitude of scattering shown in Figures 2 to 5, the amplitude shown in Figure 6 is approximately two orders of magnitude smaller. This is because the surface area inside the fracture simulated by the second model is roughly two orders of magnitude smaller than the one in the first model, but still contains the same inner medium. This makes the fracture much more rigid than the one simulated by the first model and leads to much less scattered energy. Therefore, choosing the proper parameters and models that could best describe the actual fractures in reservoirs is critical in the forward modeling as it greatly affects the simulation results. Figure 7 shows the radiation pattern for a 50 Hz incident wave, which is similar to the one shown in Figure 4 but with smaller amplitude.

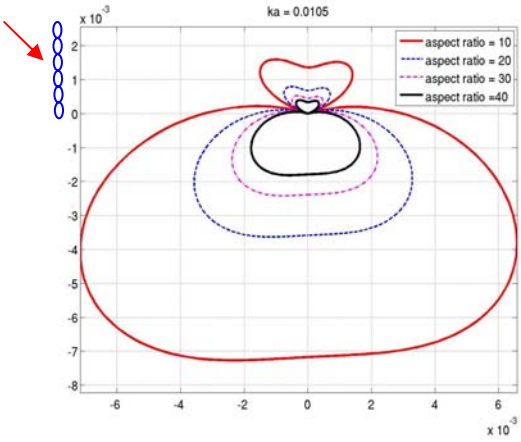

Figure 7 Similar to Figure 4, but for 50 Hz frequency

Conclusions

In this paper, we propose two physical models for a 2D fracture and then calculate its scattering pattern for different sizes, and impendence contrasts and incident wave frequency. It is found that forward scattering is much stronger than the backward scattering. As frequency decreases, scattering amplitude decreases and the directionality of the radiation pattern diminishes. Since the fracture based on the second model has smaller inside surface area and is much more rigid, its scattering amplitude is much smaller than the one based on the first model.

Acknowledgements

This work was funded by the Eni Multiscale Reservoir Science Project within the Eni-MIT Energy Initiative Founding Member Program. Tianrun Chen was supported by an ERL Founding Member postdoctoral fellowship.

References

Brown. S., and C. Scholz, 1985, Closure of random elastic surfaces in contact, *Journal of Geophysical Research*, **90**, 5531–5545

Sevostianov. I., and M. Kachanov, 2008, Normal and tangential compliances of interface of rough surfaces with contacts of elliptic shape, *International Journal of Solids and Structures*, **45**, 2723–2736.

Prioul. R and J. Jocker, 2009. Rough contacting surfaces: Similarities and differences with traction-free cracks, *SEG Expanded Abstracts* **28**, 3436

Schoenberg, M., 1980, Elastic wave behavior across linear slip interfaces, *Journal of the Acoustical Society of America*, **68**, 1516–1521.

Coates. R. T., and M. Schoenberg., 1994, Finite-difference modeling of faults and fractures, *Geophysics* **60**, no. 5, 1514-5123.

Willis, M. E., D. Burns, R. Rao, B. Minsley, M.N. Toksoz, and L. Vetri, 2006. Spatial orientation and distribution of reservoir fractures from scattered seismic energy, *Geophysics* **71**, no. 5, 43-51

Stratton. J. A., Electromagnetic Theory, *IEEE Press series on electromagnetic wave theory*, IEEE Press, c2007

Burke, J. E., and V. Twersky., 1963, On scattering of waves by an elliptic cylinder and by a semielliptic protuberance on a ground plane, *Journal of the Optical Society of America*, **54**, 732–744.

Burke, J. E., 1964, Low-frequency approximations for scattering by penetrable elliptic cylinders, *Journal of the Acoustical Society of America*, **36**, 2059–2070.